Prepared for The International Conference on
Interfaces, Melbourne, Australia,
August 18-22, 1969

UCRL-18795
Preprint

cy. 2

THE PRACTICAL ASPECTS OF SINTERING

RECEIVED
LAWRENCE
RADIATION LABORATORY
APR 7 1969
LIBRARY AND
DOCUMENTS SECTION

Robert B. Atkin and Richard M. Fulrath

February 1969

AEC Contract No. W-7405-eng-48

TWO-WEEK LOAN COPY

This is a Library Circulating Copy which may be borrowed for two weeks. For a personal retention copy, call Tech. Info. Division, Ext. 5545

LAWRENCE RADIATION LABORATORY
UNIVERSITY of CALIFORNIA BERKELEY

UCRL-18795
cy. 2

DISCLAIMER

This document was prepared as an account of work sponsored by the United States Government. While this document is believed to contain correct information, neither the United States Government nor any agency thereof, nor the Regents of the University of California, nor any of their employees, makes any warranty, express or implied, or assumes any legal responsibility for the accuracy, completeness, or usefulness of any information, apparatus, product, or process disclosed, or represents that its use would not infringe privately owned rights. Reference herein to any specific commercial product, process, or service by its trade name, trademark, manufacturer, or otherwise, does not necessarily constitute or imply its endorsement, recommendation, or favoring by the United States Government or any agency thereof, or the Regents of the University of California. The views and opinions of authors expressed herein do not necessarily state or reflect those of the United States Government or any agency thereof or the Regents of the University of California.

THE PRACTICAL ASPECTS OF SINTERING

Robert B. Atkin and Richard M. Fulrath

Inorganic Materials Research Division, Lawrence Radiation Laboratory,
and Department of Materials Science and Engineering,
College of Engineering, University of California,
Berkeley, California

ABSTRACT

February 1969

The state of the art in sintering is reviewed by discussing sintering of two ceramic material systems. Sintering of "high" alumina ceramics for structural application concentrates upon those factors effecting mechanical strength. Grain growth kinetics which control density and grain size are emphasized.

The sintering of ceramic materials which display piezoelectric and ferroelectric properties is dominated by additions used in doping or impurities from processing. The sintering of lead zirconate titanate with additives which are purposely added to enhance ferroelectric behavior and additives normally encountered in processing demonstrate the complexity of sintering this compound.

The authors are respectively graduate student and professor of ceramic engineering, Lawrence Radiation Laboratory, and Department of Materials Science and Engineering, University of California, Berkeley, California, 94720.

This work was done under the auspices of the United States Atomic Energy Commission.

1. Introduction

It is appropriate that this conference should include discussion of a major processing operation extensively used in the ceramic and metallurgical industries. Sintering relies on the change in interfacial energy as the driving force, therefore, the interface plays a dominant role.

This discussion is directed to the practical aspects of the sintering process and attempts to establish the current state of the art primarily in the sintering of oxide ceramics. Sintering will be assumed to mean that process in which an agglomeration of powder particles are heat treated at high temperature to achieve either densification of the compact or to develop mechanical strength in the compact. In ceramics and in most powder metal fabrication processes where sintering is used, it is densification that is desired. In extractive metallurgy where pelletizing and sintering are used to prepare more readily handled ores, the emphasis is placed on developing mechanical strength with maximum surface area in the pellet. In general, the sintering process is used to achieve a polycrystalline shape because of the economies compared to other fabrication techniques. This economic factor in fabrication of ceramic materials has prompted considerable interest in studying the mechanisms of sintering of ceramics. The current trend in all phases of the ceramic industry is to achieve the optimum microstructure of the ceramic material for its service environment. Again the mechanisms of sintering are of interest because they determine to a large degree the microstructure developed, which in turn is responsible for the properties exhibited by the ceramic.

2. Sintering Mechanisms

In spite of the extensive research activity on the mechanisms involved in the sintering process, we are still severely limited in predicting the sintering behavior of a specific material. Thümmler and Thomma [1] recently reviewed the sintering process including the current concepts of sintering mechanisms. It is apparent from their review that our present ability to characterize powders is one of the most serious limitations in predicting sintering behavior.

Sintering of powders is generally divided into two major areas. The first considers material transport without the presence of a liquid phase and the second allows a liquid phase.

(a) Solid State Sintering

Without a liquid phase present, material may be transported by evaporation-condensation, surface diffusion, volume diffusion, and viscous or plastic flow. It is generally accepted that only the latter two lead to densification and, therefore, are of primary interest in sintering oxide ceramics.

Starting with models composed of spherical particles and using appropriate material transport paths, Kuczynski [2] and later Coble [3] developed relations for the diffusion controlled densification process in sintering. The densification rate according to Coble for volume diffusion after an initial stage of neck growth and development of an interconnected network of cylindrical pores becomes

$$\frac{dP}{dt} = N\left(\frac{D\gamma\Omega}{\ell^3 kT}\right) \qquad (1)$$

where

P = fractional porosity

t = time

D = diffusion constant of the rate determining species

γ = solid-vapor surface energy

Ω = vacancy volume

k = Boltzman constant

T = temperature

ℓ = a dimension related to the grain size

N = constant depending on the pore geometry.

MacKenzie and Shuttleworth [4] treated densification by viscous or plastic flow and related the densification rate of the solid to the solid-vapor surface energy, γ, a Newtonian or Bingham solid viscosity, η, and the pores per unit volume, n. For sintering powders n would be determined by the initial particle size in the compact.

In the models developed by MacKenzie and Shuttleworth, a closed pore geometry is assumed. The surface energy of the pore leads to the equivalence of an externally applied pressure to the compact. This pressure should not be developed with open porosity that is generally encountered below 90 to 95 percent of the theoretical density.

Frenkel [5] developed a model for viscous flow in the initial stage of sintering (neck growth between particles) which was found by Kingery and Berg [6] applicable to sintering glass spheres. Other than glass sintered in the initial stages the viscous or plastic flow models have not been experimentally verified to be applicable to sintering ceramics. Solid stage sintering, therefore, has concentrated on mass transport by

a diffusion process.

The techniques of studying the sintering process have generally concentrated on obtaining densification-time relationships at various temperatures and from this data and grain size determinations calculate the shrinkage-time dependence. Calculations of a diffusivity and the activation energy for diffusion through the use of equation (1) can also be made. Corrections to equation (1) must be made for grain boundary diffusion if it is the rate limiting process [7]. For oxide ceramics the diffusivity and activation energy so determined in sintering studies have shown considerable variation for different investigators examining the same material. However, the model has confirmed the mechanism although there is still debate as to the details such as diffusion paths.

Equation (1) establishes directions to improve sintering. First, the powder to be sintered should have the smallest particle size possible consistent with the processing operations prior to sintering. Second, the grain size change during sintering should be minimized. Third, enhancement of diffusivity where possible will increase densification rates. It is assumed that for a given material one has little control over the solid-vapor surface energy or vacancy volume. Other variables in the sintering process will also be discussed later.

(b) Sintering with a Liquid Phase

Although most commercial ceramic materials produced contain a liquid phase during the sintering operation, little attention has been given to this mechanism. Kingery [8] has presented models for liquid phase sintering where the liquid does not penetrate the boundary between two crystalline particles and where complete wetting of the crystalline

phase occurs. These conditions are achieved where $\gamma_{SL} > \frac{\gamma_{SS}}{2}$ and $\gamma_{SL} < \frac{\gamma_{SS}}{2}$, respectively.

In the case where incomplete wetting of the solid occurs, the liquid phase may assist in particle rearrangement, but after this step, material transport would be either by plastic flow or a solution-precipitation process similar to evaporization-condensation.

In the case where complete wetting occurs, Kingery [9] has derived shrinkage-time relationships for the rate controlling step in the solution-precipitation region as being either diffusion through the liquid or the phase boundary reaction. In Kingery's models and those of others, the amount of liquid necessary for liquid phase sintering kinetics is unknown. White [10] has raised objections to the Kingery model regarding complete penetration of the liquid phase between grain contacts pointing out that measurement of the dihedral angle between solid-solid-liquid contacts indicate incomplete penetration of the liquid phase while densification is still proceeding. Both the rate of densification and grain growth rate are dihedral angle dependent which is contrary to Kingery's model.

(c) Comparison of Models for Sintering

Accepting that for oxide ceramics liquid phase sintering or diffusion controlled solid state sintering are appropriate models, one can compare the shrinkage-time relation predicted by the two models from the equation

$$\frac{\Delta L}{Lo} \propto k\ t^{x} \qquad (2)$$

where

$\frac{\Delta L}{Lo}$ = observed linear shrinkage

k = a constant depending on the mechanism and including a grain size parameter

t = time of isothermal sintering.

Table I

Diffusion and Liquid Phase Sintering Parameters

Mechanism	Time Exponent (Eq. 2)	Reference
Bulk diffusion	0.4 to 0.5	[2, 3, 6]
Grain boundary diffusion	0.3	[7]
Liquid phase (diffusion control)	0.3	[9]
Liquid phase (solution rate control)	0.5	[9]

As shown in Table I, the use log shrinkage-log time plots to evaluate mechanisms is useless. Therefore, there is a strong incentive to evaluate the grain size dependence, observed diffusivities, and the activation energy associated with the process. Microstructure analysis is also necessary and new tools such as the scanning electron microscope and electron microprobe are playing an important role in assisting in interpretation of mechanisms.

3. Sintering Commercial Ceramics

Aluminum oxide, today, is probably the most widely used technical ceramic. Its applications range from polycrystalline nearly transparent sodium lamp envelopes to alumina porcelain grinding media. The industry

produces a range of materials all under the name high alumina ceramics. They are classified according to the alumina content [11]. The alumina content can range from 80 w/o to better than 99.8 w/o. Obviously, the production processing from raw materials to finished product is varied for each type material.

In aluminas with the alumina content between 80 and 95 w/o a silicous liquid phase containing alkali or alkaline earth oxides to flux the alumina-silica glass forming oxides leads to liquid phase sintering. The final material usually is composed of a primary crystalline phase, Al_2O_3, and secondary crystalline phases formed during sintering or by crystallization from the liquid phase during cooling from the sintering temperature. Also present is a glassy phase and either or both open and closed porosity. All these features are usually easily observable by optical microscopy.

The use of these materials is primarily limited to temperatures dictated by the characteristics of the glass phase. Their mechanical and physical properties at low temperatures are quite dependent on the microstructure produced during sintering. Manufacture, including sintering, of these ceramics is directed to producing a reproducible material at the lowest possible cost. Grinding to achieve dimensional tolerance after sintering is economically prohibitive so the total firing shrinkage of the compacted shape is of primary importance. Process steps from mixing raw materials, compacting and forming shapes, and sintering variables all contribute to the densification during sintering. It is not surprising that few studies of sintering such complex materials have been reported.

Individual ceramic producers in evaluating their existing or proposed new facilities and raw materials extensively vary process parameters including sintering parameters of time and temperature to establish the process limitations. Seldom are the results of these investigations published although they would contribute significantly to evaluating liquid phase sintering.

When the alumina content is above 95 w/o one should expect a change at some composition from liquid phase sintering to solid state mechanisms. This transition would be expected to be extremely sensitive to the exact nature and content of the other atomic species present. It becomes increasingly difficult to identify the phase relations as the alumina content increases. Ions may be in solid solution, concentrated at grain boundaries, or contribute to secondary phase formation which may be liquid or crystalline at the sintering temperature. At present, our analytical tools such as optical and electron microscopy, X-ray diffraction, and electron microprobe are not able to distinguish all the details necessary for analysis.

As an example of the complexity of these sintered materials, Edwards [12] in studying helium gas permeation through both commercial 94 w/o and a 99.5 w/o alumina ceramic, found that although the lower alumina content material had a permeation coefficient approximately 15 times that of the higher alumina material, the activation energy for permeation was the same for both. This activation energy was close to that to be expected for a silicate glass and much lower than that expected for permeation through crystalline Al_2O_3. No glassy phase could be detected by microscopic analysis in the higher purity ceramic. The lower alumina

content ceramic had an easily identifiable glass phase present. Therefore, one might speculate that the observed activation energy may be associated with helium permeation along grain boundaries and that the grain boundary structure is disordered analogous to the structure in a silicate glass.

To date, our ability to classify the effect of impurities on sintering is at best emperical. Brockway and associates [13] in reviewing firing processes point to the fact that the divergence of results with similar additives by different investigators makes it meaningless to interpret sintering phenomena in any system not completely characterized.

In developing the techniques of solid state sintering alumina to a nearly transparent polycrystalline material, Coble [3] found an MgO additive below the solubility limit would suppress discontinuous grain growth in sintering a high purity submicron particle size alumina. With the MgO addition preventing abnormal grain boundary motion and subsequent entrapment of pores within grains and by control of the sintering atmosphere to prevent non-diffusable gases being trapped in closed pores, sintering to near theoretical density was achieved. Unlike many ceramic materials such as UO_2, alumina apparently does not show a stoichiometry effect when sintered in either oxygen or dry hydrogen. Although such an effect has been reported by others [13], Coble [3] found no difference in sintering in either atmosphere.

In solid state sintering processes with high purity materials, attention is now focused on the interface between grains. Controlling discontinuous and normal grain growth is one of the key factors in sintering to densities near theoretical. Burke [14] in reviewing grain growth

in ceramics suggests that an addition which decreases grain boundary mobility without completely preventing grain growth can inhibit discontinuous grain growth.

Nicholson [15] has examined grain growth in MgO. He reported than an addition of 0.05 at./0 V_2O_5 results in grain growth kinetics that are similar to those when a detectable volume of liquid is present. This again points to the importance of the interface between grains.

Pores, themselves, may influence grain growth kinetics and Nichols [16] has recently proposed new mechanisms for grain growth in porous compacts. In sintering one would expect that pores would influence the grain growth kinetics. Nichols in analyzing grain growth in porous Al_2O_3 and UO_2 suggests that the observed cubic growth law is best described by material transport through the vapor phase where the pressure in the pore is given by the Kelvin equation. Pores, therefore, can control grain growth kinetics. Where the pore influence stops and the boundary mobility controls grain growth is a topic of current interest.

In "solid state" sintering grain growth can be controlled by pores, additions below solubility limits, and additions that form undetectable second phases. It is obvious that studies of sintering where grain growth is an important parameter will require extensive improvement in our present abilities to characterize the nature of the interface between grains in a compact.

4. Sintering Ferroelectric Ceramics

(a) Introduction

While alumina dominates the application of ceramics to structural problems, the ferroelectric and piezoelectric ceramics of current interest

are compositions in the lead titanate-lead zirconate system (PT-PZ). Both end members have cubic perovskite structures above their Curie temperatures and the system forms a continuous solid solution series. Below the Curie temperature, where piezoelectric and ferroelectric activity is observed, two primary crystal structures are present. Above 47 mole/O PT the low temperature structure is tetragonal while the ferroelectric compositions with lower PT content have a rhombohedral structure. Near the PZ end of the diagram complex structures and anti-ferroelectricity are observed. The most interesting ferroelectric and piezoelectric behavior is observed near the rhombohedral-tetragonal phase boundary.

The studies reported on this system have mainly concentrated on the effect of dopants added to the basic lead zirconate titanate (PZT) to modify the ferro-and piezo-electric properties. The fabrication of dense ceramic shapes of thermally reacted PbO, ZrO_2, TiO_2, and doping additions has primarily been by hot pressing [17]. This method is used because of the high lead oxide vapor pressure above compositions in the system (near 1 Torr. at 1100°C).

Iwasaki [18] reported that undoped PZT of less than 20 mole/O PZ sintered by a volume diffusion mechanism and compositions of greater than 20 mole/O PZ sintered by a surface diffusion mechanism. It is not clear whether this was meant to be grain boundary diffusion since surface diffusion should not lead to densification.

Pryor [19] chose one undoped composition of 60 mole/O PT for sintering studies. He determined that after forming the PZT compound by calcination and grinding the lightly sintered pellets with high alumina media, sufficient Al_2O_3 and SiO_2 impurities were picked up to significantly

effect the densification during sintering. Further studies on material ground in an acrylic container with acrylic balls showed that as little as 0.4 wt/0 Al_2O_3 could increase the density of material sintered at 1200°C for 1-1/2 hours from 82 to 92 percent of theoretical density. SiO_2 additions of the same percentage gave less dramatic results but followed the same pattern.

Even more significant results were obtained when the as sintered surfaces were examined by scanning electron microscopy. The samples which had an Al_2O_3 additive showed rounded grains indicative of liquid phase sintering with a grain size approximately one tenth that of the material with no addition or with a SiO_2 addition. The addition of SiO_2 caused the appearance of a very small grain size secondary phase concentrated in the grain boundaries. X-ray analysis and optical microscopy on etched polished sections showed little difference in the three materials. Electron microprobe analysis indicated that a lead aluminate was present in selected pockets when the additive was Al_2O_3 and a lead zirconate silicate when SiO_2 was added. The analysis could not be extended to grain boundaries due to the limits of resolution of electron microprobe.

Following Pryor's investigation, a comprehensive study on sintering a PZT composition was undertaken. The results are presented here to demonstrate how various additions or solid solution dopants can alter sintering kinetics, grain growth characteristics, and ceramic ferroelectric and piezoelectric properties. Also, the ferroelectric properties along with scanning electron microscope analysis combined with conventional densification-time relations were used in interpretation of the data.

Pryor had determined that Al_2O_3 and SiO_2 contamination could occur during conventional ceramic processing. These two materials were chosen as additions to unmodified and solid solution doped PZT compositions.

Both bismuth and niobium are standard commercial doping additions used to alter ferroelectric properties of PZT ceramics. They were chosen to determine their effect on sintering and on the subsequent electrical properties. Table II gives the ionic radii of the various ions expected to be present in unmodified, doped, and addition modified PZT according to Ahrens as tabulated by Azaroff [20].

Table II

Six-Fold Coordination Radii of Interest in ABO_3 Doped and Addition Modified Ceramics

Ion	Ionic Radii (Å)	Predicted Position
$O^{=}$	1.40	O site
Pb^{+2}	1.20	A site
Ti^{+4}	0.68	B site
Zr^{+4}	0.79	B site
Bi^{+3}	0.96	A site
Nb^{+5}	0.69	B site
Al^{+3}	0.51	No solid solution
Si^{+4}	0.42	No solid solution

The perovskite unit cell consists of 8 "A" ions at the corners of a cube with oxygen ions occupying the cube faces. The "B" ion is placed

in the center of the cube. Ferroelectricity is considered to be primarily due to the "B" ion being too small for the octahedral hole created by the oxygen ions. This misfit increases the covalent nature of the bonding with a resultant distortion of the cubic unit cell to either a rhombohedral or tetragonal structure. Movement of ferroelectric domain walls to cause either 90° polarization or 180° polarization reorientation is then possible in an individual crystal with the application of an electric field. The ease of domain boundary movement will determine whether a ferroelectric is "hard" or "soft" analogous to ferromagnetic behavior.

In the perovskite structure for ideal cubic packing, the "A" cation should have the same ionic radii as the oxygen anion to achieve cubic close packing. The "B" cation would then fill the octahedral hole in the structure and balance the change.

As shown in Table II, Pb^{+2} is approximately 14 percent smaller than the oxygen ion. Because of this misfit and polarizability of the lead and oxygen ions, it is expected that an interaction between the polarization of the central cation and the "A" cation would lead to enhanced ferroelectricity. This is apparently the case with lead titanate which shows one of the highest Curie temperatures known. Unfortunately, the cubic-tetragonal phase transformation in lead titanate results in a tetragonal c/a ratio of 1.06 and in polycrystalline materials the lattice strain on transformation is sufficient to mechanically shatter the ceramic. When titanium is replaced with zirconium (a larger cation) the c/a ratio decreases. Near the rhombohedral-tetragonal phase boundary the ratio is reduced to the extent that the cubic-tetragonal transformation may

occur without destruction of polycrystalline ceramics.

(b) Experimental Procedures

The basic composition selected for this study was near the rhombohedral-tetragonal phase boundary but in the tetragonal phase stability region $\{Pb\ (Zr_{.53}\ Ti_{.47})\ O_3\}$.

(i) Preparation of Compacts for Sintering

High purity lead oxide, titanium dioxide, hafnium free zirconium dioxide, bismuth trioxide, and niobium pentoxide were used to compound batches with the compositions shown in Table III. Bismuth was assumed to substitute for lead as a +3 ion because of the thermodynamic instability of the pentavalent state. Every two substutional Bi ions should create one lead vacancy. Niobium was predicted to enter the octahedral "B" site as a +5 ion and similarly produce one lead vacancy for every two niobium ions.

Table III

Basic and Solid Solution Compositions

Dopant	Compound Formula Assumed
None	$Pb\ (Zr_{.53}Ti_{.47})\ O_3$
Niobium	$Pb_{.99}\ \square_{.01}\ (Zr_{.53}Ti_{.47})_{.98}\ Nb_{.02}\ O_3$
Bismuth	$Pb_{.97}\ Bi_{.02}\ \square_{.01}\ (Zr_{.53}Ti_{.47})\ O_3$
Niobium + Bismuth	$Pb_{.96}\ Bi_{.02}\ \square_{.02}\ (Zr_{.53}Ti_{.47})_{.98}\ Nb_{.02}\ O_3$

$\square$ indicates lead vacancy

The oxides were weighed directly into a Neoprene lined ball mill. Teflon cylinders were used as mixing media and isopropyl as the suspending liquid. An individual batch was vibratory milled four hours, then rotary milled for 20 hours. After this mixing treatment, the alcohol was evaporated at 70°C. The mixed material was compacted into 2" diameter by 2" high pellets in a plastic lined die by pressing at 4000 psi. The pellets were packed in unconsolidated material from the same batch and calcined in a covered platinum crucible at 850°C for 20 hours. X-ray analysis indicated complete reaction to tetragonal PZT. The calcined material was lightly sintered with an indicated particle size of 4 to 6 microns as measured by an air permeation sub sieve size analyzer.

The calcined pellets were crushed with an acrylic mortar and pestal, then vibratory milled 10 hours in a low ash rubber lined mill with acrylic grinding media. The organic material was removed by air oxidation at 400°C for 12 hours. The particle size of all compositions at this stage was between 1.4 and 1.6 microns.

Spectrographic analysis indicated that all compositions had approximately 0.05 wt/0 Al_2O_3, 0.02 wt/0 each of SiO_2 and CaO, and 0.002 wt/0 MgO. These impurities were approximately what would be expected from the original oxides used in compounding the compositions.

Silica and alumina additions of 0.4 wt/0 each were individually made to 80 gram batches of each of the four compositions. The alumina was added as an aqueous solution of aluminum nitrate. The silica was added as an aqueous suspension of colloidal silica. Distilled water was added to the batches with no additions (2.5 wt/0) to aid in cold pressing. Fifteen pellets were cold pressed from each of the 12 batches in a 0.75"

dia. steel die at 60,000 psi.

All pellets were presintered on platinum covered platinum sheets at 800°C for one hour. This presintering decomposed any aluminum nitrate present and increased the green strength. After presintering the pellets were stored in a desiccator. All green densities were between 65 and 70 percent of the theoretical density.

(ii) Sintering Procedures

The high lead oxide vapor pressure required that an equilibrium atmosphere be established around each pellet during sintering. The sintering configuration is shown in Figure 1. All pellets were packed in an undoped $Pb(Zr_{.53}Ti_{.47})O_3$ powder that had not been milled. The loose unconsolidated packing powder did not sinter appreciably, so pellets were easily removed from it on completion of a sintering run.

All sintering runs were made under one atmosphere of oxygen to suppress anion vacancy formation. The procedure was identical for each sintering run. After the sintering crucible was loaded into place the furnace volume was evacuated for one hour. Oxygen was then introduced and a flowing system was maintained during the sintering run. The furnace was heated at 300°C/hr to the sintering temperature of 1200°C, held for the required time, then cooled at 300°C/hr to 800°C. From 800°C to room temperature the furnace was allowed to follow its natural cooling rate.

(iii) Analytical Measurements

Densities of sintered pellets were measured by mercury displacement. The as fired surfaces (thermally etched) and fractured surfaces were examined with the scanning electron microscope. Approximately 100Å of

aluminum was vacuum evaporated on the surface to allow charge dissipation. Optical microscope observations were made on both polished and polished and etched surfaces. Due to the superior micrographs obtained on the scanning electron microscope, all grain size analyses were made on these micrographs using the intercept method. The reported values are 1.5 times the average cord length.

Ferroelectric hysteresis measurements were made on the sintered disks. Electrodes 0.75 cm in diameter were formed on the specimens with an air drying silver paint. The samples were approximately 0.2 cm thick. The electrical measurements were made by applying a slow triangular wave form (period approximately 90 sec, peak field of 70 volts/mil) to the specimen and monitoring the accumulated charge (polarization) with an integrating capacitor. The loops were plotted with an X-Y recorder.

Piezoelectric measurements were made using the same power supply as used for the ferroelectric measurements. The sample extension was measured parallel to the applied electric field by a linear differential transformer. These loops were also recorded on an X-Y recorder.

(c) Experimental Results

During the heating to the sintering temperature, some densification occurred. In order to allow for this initial sintering and to assure thermal equilibrium, a 20 minute hold at 1200°C was selected as the initial time from which the density time relations for isothermal sintering were to be determined.

Each of the twelve compositions achieved a different initial density. It was noted that the dopant had a marked effect on this initial density with or without the Al_2O_3 or SiO_2 additives. By plotting the initial

density against the assumed lead cation vacancy concentration plus the bismuth dopant level, a reasonable relation was obtained for all twelve compositions. (Figure 2).

The four compositions containing no alumina or silica additive were sintered for various times and the density plotted against the square root of the reduced time $(t-t_o)$ where t_o is 20 minutes. The data shown in Figure 3 indicates that the sintering can be described by the relation:

$$\rho = \rho o + K\ (t-t_o)^{1/2} \qquad (3)$$

The slope, K, was approximately the same for the doped material. The undoped material exhibited a lower slope. Deviation from the relation in equation (1) was only observed for densities greater than 98% of theoretical.

The undoped and doped compositions containing alumina or silica additions sintered according to a cube root time dependence.

$$\rho = \rho o + K^1\ (t-t_o)^{1/3} \qquad (4)$$

The data for compositions with a silica additive are shown in Figure 4 and the compositions with an alumina additive in Figure 5. Six of the eight compositions followed the relation in equation (4) while the other two achieved such high initial densities that their sintering was essentially complete. These two compositions, however, did follow the kinetics of equation (4) when sintered at 1170°C.

The grain growth kinetics did not appear to follow any trend so the data are plotted in Figures 6 and 7 for all the compositions except the bismuth plus niobium doped. These measurements were made on the as sintered surfaces but were found comparable to value obtained by optical

microscopy of interior grains.

Typical microstructures of as sintered surfaces observed by scanning electron microscopy are shown in Figures 8, 9 and 10. The rounded grains (Figure 8) are characteristic of undoped PZT (alumina and no additive) and niobium doped compositions (alumina, silica, and no additive).

Figure 9 is typical of the flat surfaces with slightly etched grain boundaries shown by bismuth doped materials (alumina, silica, and no additions) and undoped material containing silica. These microstructures were consistently observed (5 to 8 specimens for each composition) and were independent of sintering time. Therefore, the microstructure was dependent on composition and independent of grain size and density.

Figure 10 shows the grain boundary secondary phase observed by Pryor [19] in compositions containing silica.

The ferroelectric loops observed are shown in Figure 11 and actual ferroelectric parameters given in Table IV.

Table IV

Observed Ferroelectric Properties

Composition		Ferroelectric Properties			
Dopant	Addition	Loop Shape (Fig. 12)	E_c Volts/Mil	P_r μ coul/cm^2	P_s μ coul/cm^2
None	None	Intrinsic	17	10	23
	Al	Anti-ferro	-	-	-
	Si	Broad	51	26	38
Nb	None	Square	21	39	43
	Al	Intrinsic	26	15	22
	Si	Square	40	39	44
Bi	None	Square	23	41	48
	Al	Square	23	34	37
	Si	Square	35	42	46
Bi + Nb	None	Square	24	31	39
	Al	Square	26	35	42
	Si	Square	34	29	37

(d) Discussion of Results

The basic lead zirconate titanate composition selected for this investigation appears to follow solid state volume diffusion kinetics in sintering when no additives are present. Substitutional ions introduced to improve ferroelectric behavior increase the "A" site cation vacancies and lead to enhanced sintering. It would be expected that diffusion of +4 valent ions would be relatively slow and hence rate determining. If the diffusion path involves a two step process of a jump from the "B" site to the "A" site, then to a new "B" site, it is expected that an

increase in "A" site vacancies would enhance diffusion. This type behavior is indicated by the slopes shown in the densification time curves in Figure 3. The solid solution of the dopant ions is substantiated by the change in the ferroelectric properties. In Table IV niobium, bismuth or both develop square loops from the intrinsic loops shown by the undoped composition. Although both bismuth and niobium should have produced equal numbers of lead vacancies and given identical sintering behavior, bismuth has a more pronounced effect on the initial density.

As a counter argument, it could be proposed that at the levels of doping used in this investigation, the PZT was saturated with bismuth and the excess dopant formed a liquid phase. Bismuth oxide and lead oxide form a low melting eutectic which could assist densification prior to isothermal sintering. The mechanism of liquid phase sintering must then be solution rate controlled as proposed by Kingery [9].

Niobium, however, if present in excess of saturation, would not be expected to form a low melting liquid phase. The excess niobium would react with lead oxide vapor supplied by the packing powder and form a refractory lead niobate. Therefore, this system must actually be sintering by a solid state volume diffusion mechanism.

The grain growth kinetics shown in Figure 7 indicate a difference in the effect of bismuth and niobium with niobium suppressing grain growth much more than bismuth. Further, the sintered surfaces of bismuth doped material were observed to differ from either the undoped or niobium doped material. At present, even with additional information provided by ferroelectric measurements which are quite sensitive to lattice defects, the sintering behavior of doped materials is still debatable.

When silica is added to doped or undoped material, the densification kinetics are changed to those of liquid phase sintering (Figure 4). The initial densities follow the same pattern as the unmodified material except that they are higher (Figure 2). This could be simply the result of increasing the liquid volume at the sintering temperature. An increase in the coercive field is noted whenever silica is present. This and the observed second phase at grain boundaries (Figure 10) support the existence of a continuous grain boundary phase. The field actually applied to individual ferroelectric crystals in a ceramic would be decreased due to the large potential drop across the low dielectric constant silicate phase. This is illustrated in Figure 12. Whereas silica promotes grain growth in the undoped material, it has relatively little effect on doped compositions. The alumina addition to doped and undoped material is by far the most interesting. First, alumina suppresses the initial density (Figure 2) even though the sintering kinetics indicate liquid phase sintering. The most surprising result is the effect on the undoped materials ferroelectric behavior. The change from intrinsic to anti-ferroelectric type loop (Table IV) indicates that some Al^{+3} ions go into solid solution. The only possible site is the "B" site and such solution should decrease the lead vacancy concentration. From the ionic size of aluminum it would not be predicted that Al^{+3} could enter a site where the titanium ion is postulated to be too small. The aluminum ionic radius is nearly 25 percent smaller than titanium. This violates all crystal chemistry rules, but the evidence for substitution in the lattice is clear. In niobium doped material the effect of aluminum solution is still seen in shifting the ferroelectric loop.

The sintering kinetics of compositions with alumina additives indicate that with doped materials more alumina may enter the lattice than with undoped material and the densification rate is decreased by the reduction in liquid volume.

The grain growth kinetics are even more puzzling, whereas alumina suppresses grain growth in undoped PZT, it enhances it in niobium doped material.

The interactions of dopants and additives in the PZT system are at best qualitatively known. Liquid phases are apparently formed with extremely small impurity contents and unexpected lattice substitutions can occur. However, the understanding of such complex systems is the goal of research on sintering.

5. Summary

Two practical examples of the complexity of the sintering process have been demonstrated by the aluminum oxide and lead zirconate titanate systems. It is evident that although the subject of sintering has been extensively investigated, the development of theory has outdistanced our development of analytical tools and ability to characterize the materials we deal with. The interface between crystalline particles in a compact holds the key to the future development of our understanding of sintering.

ACKNOWLEDGMENTS

Thanks are extended to R. Unverferth and J. Lawson for experimental assistance.

The authors would also express their appreciation for the use of the scanning electron microscope within the Electronics Research Laboratory, University of California, provided under Grant No. GB-6428 from the National Science Foundation and under Grant No. GM-15536 from the National Institute of Health.

This work was done under the auspices of the United States Atomic Energy Commission.

REFERENCES

1. F. Thümmler and W. Thomma, Metallurgical Review 115, The Metals and Metallurgical Trust, 1967.
2. G. C. Kuczynski, Metals Transactions, 1949, 185, 169.
3. R. L. Coble, J. Appl. Phys., 1961, 32, 787, 793.
4. J. K. MacKenzie and R. Shuttleworth, Proc. Phys. Soc., 1949, 62, 833.
5. J. Frenkel, J. Phys. (U.S.S.R.), 1945, 9, 385.
6. W. D. Kingery and M. Berg, J. Appl. Phys., 1955, 26, 1205.
7. D. L. Johnson and I. B. Cutler, J. Am. Ceram. Soc., 1963, 46, 541.
8. W. D. Kingery, "Ceramic Fabrication Processes," New York, 1958 (John Wiley and Sons, Inc. and The Technology Press of M.I.T.).
9. W. D. Kingery, J. Appl. Phys., 1959, 30, 301.
10. J. White, Proc. Brit. Ceram. Soc., 1965, 3, 155.
11. Standards of Alumina Ceramic Manufacturers Association for High Alumina Ceramics, 2nd Edition, 1964, New York (Alumina Ceramic Manufacturers Association).
12. R. H. Edwards, M. S. Thesis, Univ. of Calif., Berkeley, 1966 (UCRL-17083).
13. M. C. Brockway, et al., U. S. Air Force Technical Report AFML-TR-65-281, 1965.
14. J. E. Burke, "Ceramic Microstructures," New York, 1968 (John Wiley and Sons, Inc.).
15. G. C. Nicholson, J. Am. Ceram. Soc., 1965, 48, 525.
16. F. A. Nichols, J. Appl. Phys., 1966, 37, 4599.
17. G. Haertling, Am. Ceram. Soc. Bull., 1964, 43, 875.

18. H. Iwaski, Jap. J. Appl. Phys., 1965, 4, 190.

19. G. A. Pryor, M. S. Thesis, Univ. of Calif., Berkeley, 1968 (UCRL-18191).

20. L. V. Azároff, "Introduction to Solids," New York, 1960 (McGraw-Hill Book Company).

FIGURE CAPTIONS

Figure 1. The sintering configuration for sintering in an equilibrium vapor pressure.

Figure 2. The initial density achieved after sintering 20 min. at 1200°C vs. the lead vacancy plus bismuth concentration. X = the at./0 bismuth and Y = the at./0 niobium added to the basic composition.

Figure 3. Density vs. the reduced time for isothermal sintering for compositions with no additives.

Figure 4. Density vs. the reduced time for isothermal sintering for compositions with a silica additive.

Figure 5. Density vs. the reduced time for isothermal sintering for compositions with an alumina additive.

Figure 6. Sintered grain size vs. sintering time for compositions with no dopants.

Figure 7. Sintered grain size vs. sintering time for bismuth and niobium doped compositions.

Figure 8. Scanning electron micrograph of undoped material with no additives sintered 20 minutes at 1200°C. Relative density is 78 percent.

Figure 9. Scanning electron micrograph of a bismuth doped material with no additive sintered 120 minutes at 1200°C. Relative density is 98.9 percent.

Figure 10. Scanning electron micrograph of undoped material with a silica additive sintered 720 minutes at 1200°C. Relative density is 86.6 percent.

Figure 11. Typical ferroelectric loops observed. (See Table IV).

Figure 12. The physical and dielectric model for a two phase ceramic with ferroelectric crystals separated by a grain boundary phase.

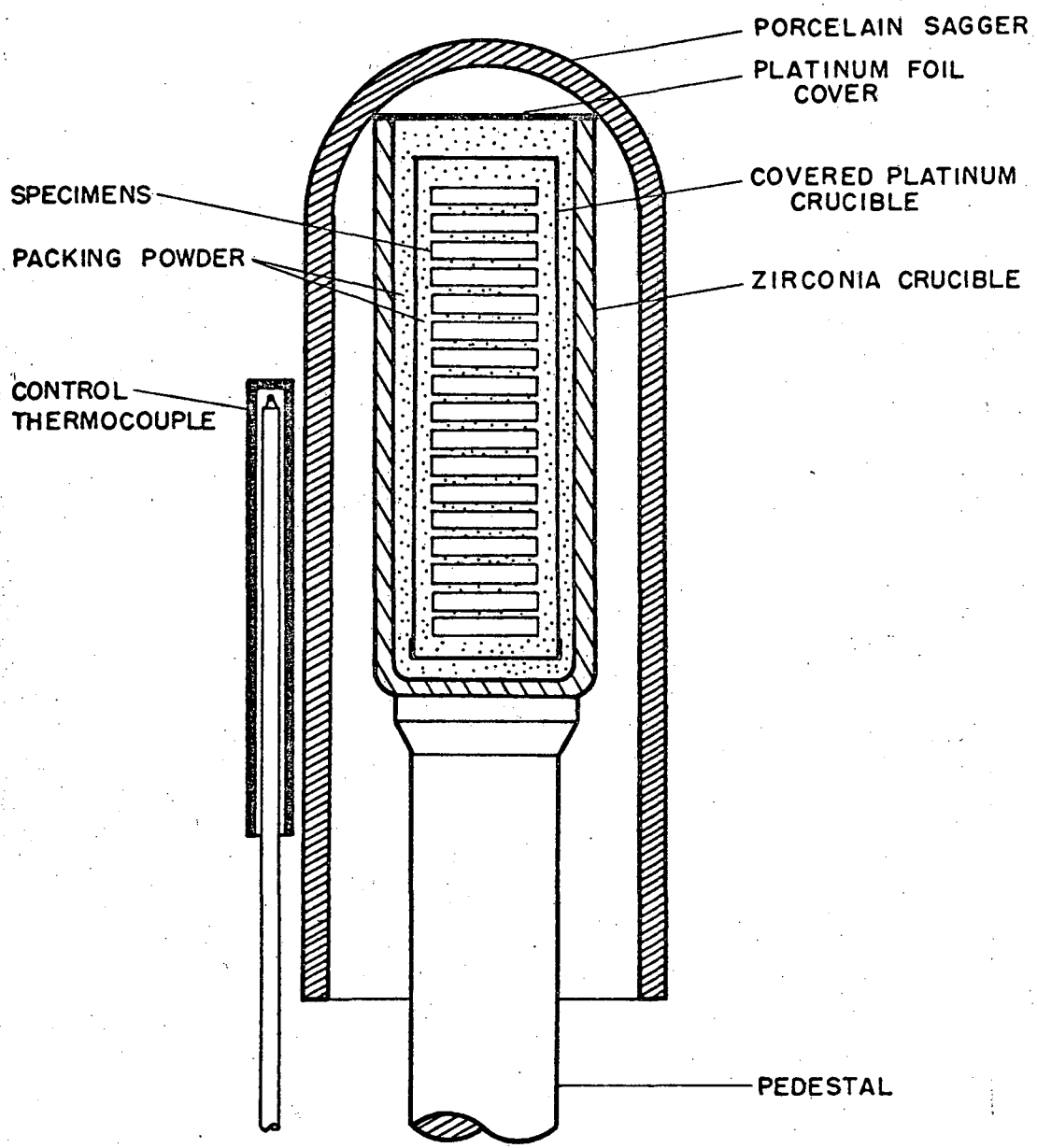

XBL 6812-6358

Fig. 1

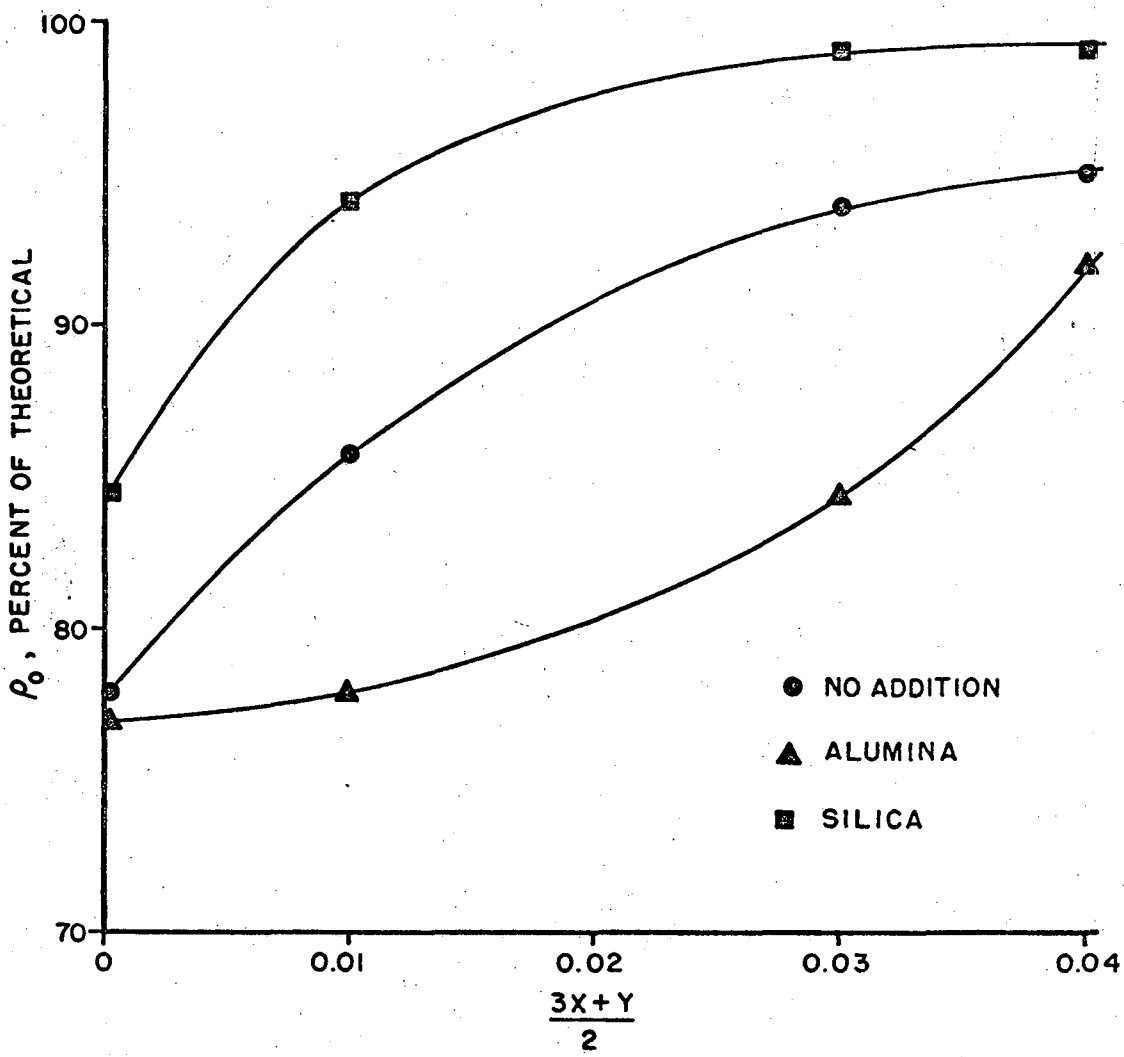

XBL 6812-6359

Fig. 2

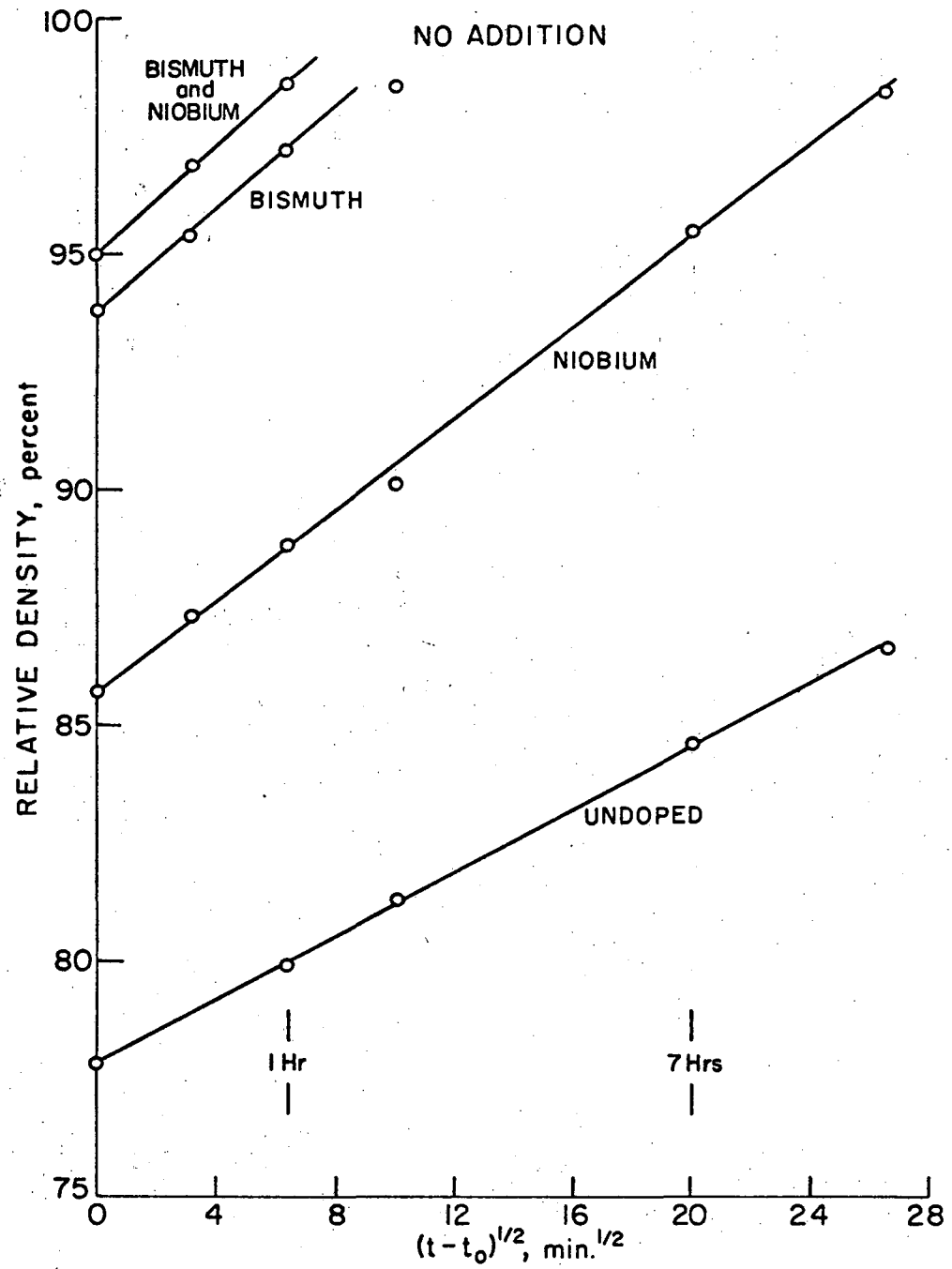

XBL 6812-6360

Fig. 3

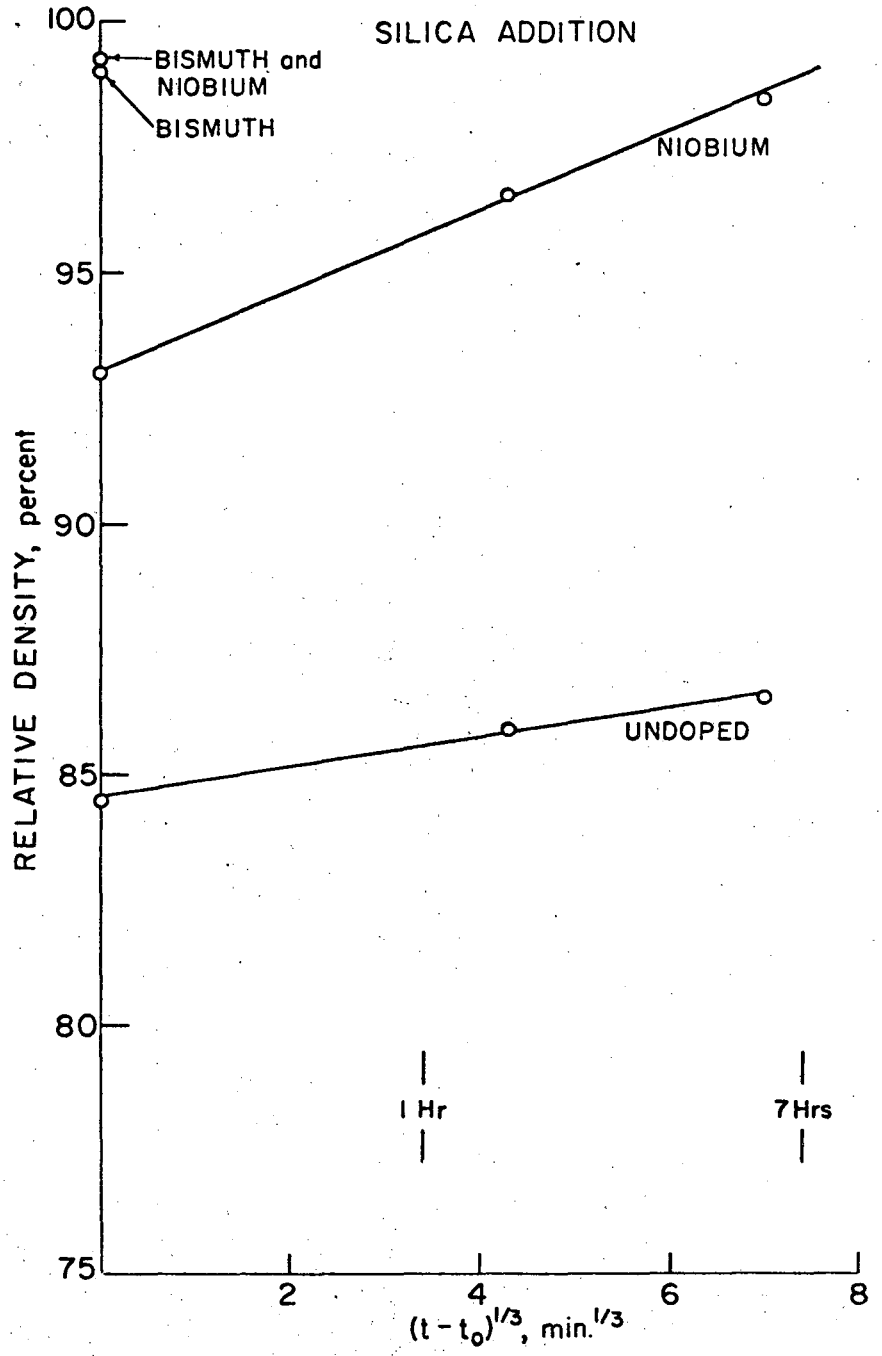

XBL 6812-6362

Fig. 4

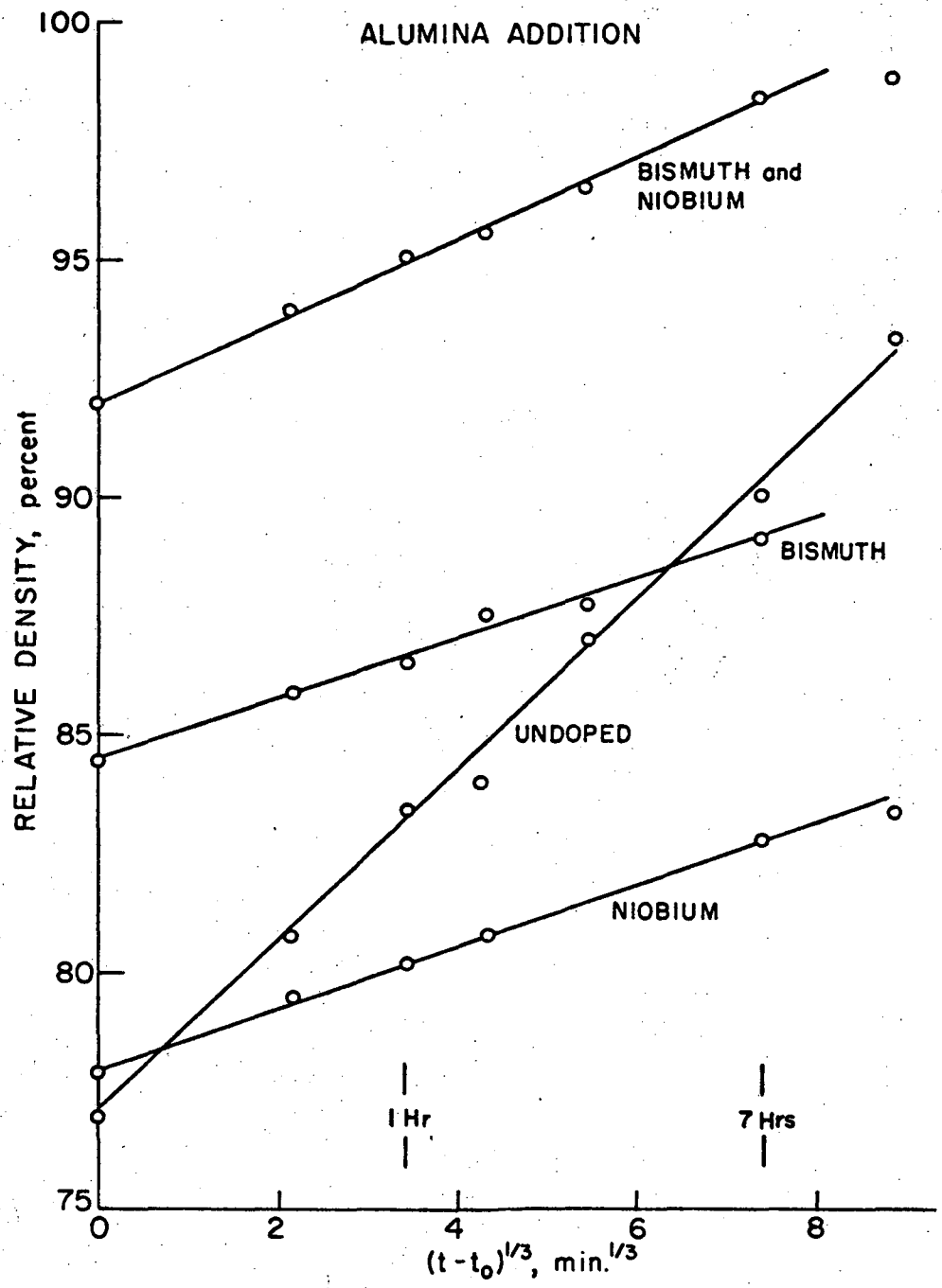

XBL 6812-6361

Fig. 5

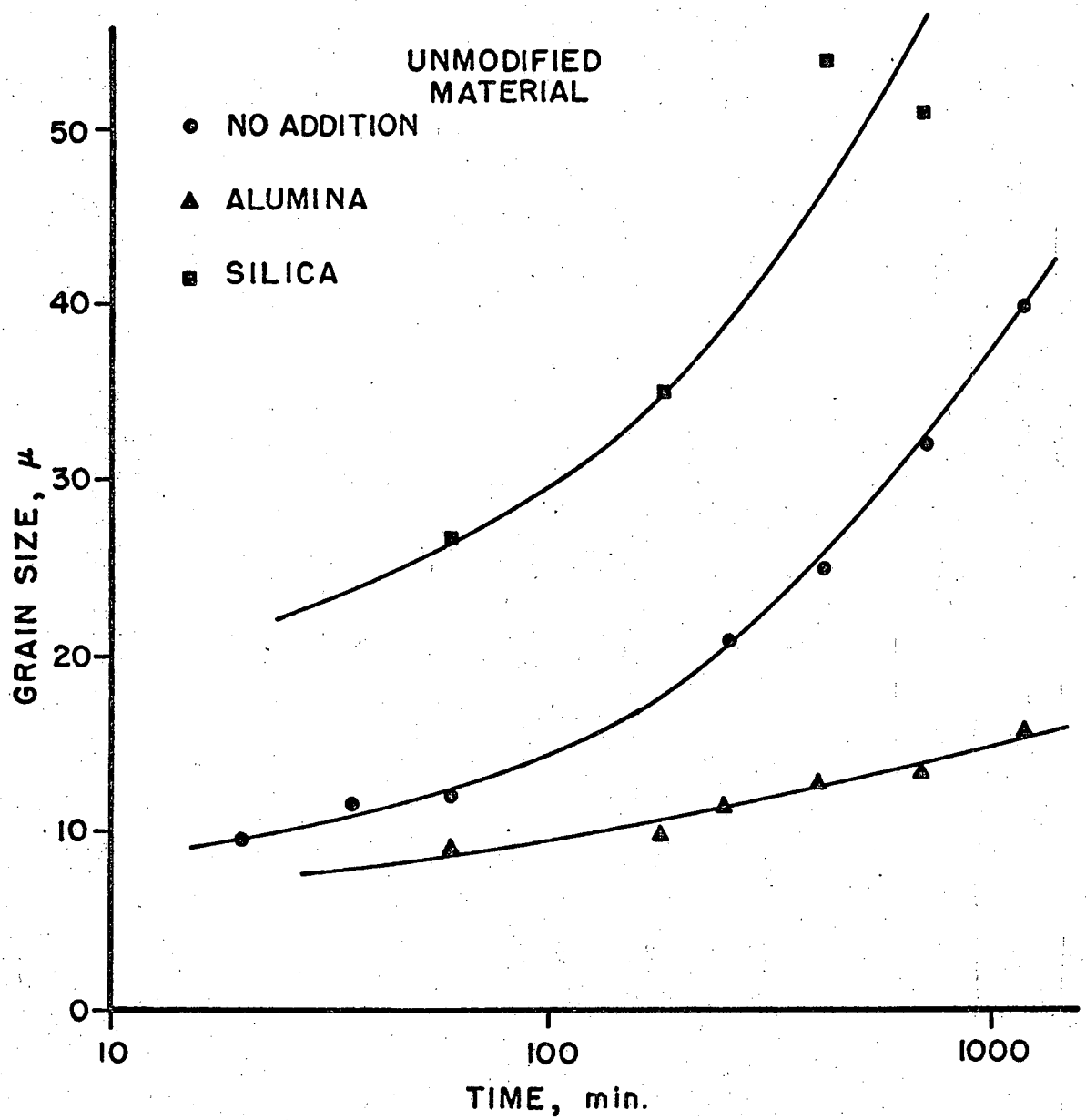

XBL 6812-6363

Fig. 6

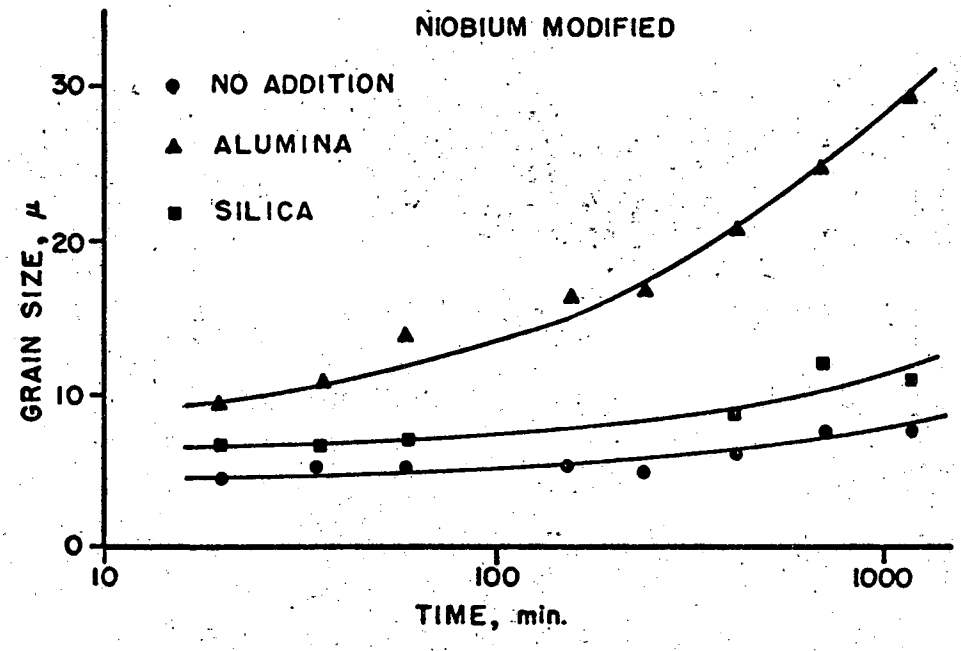

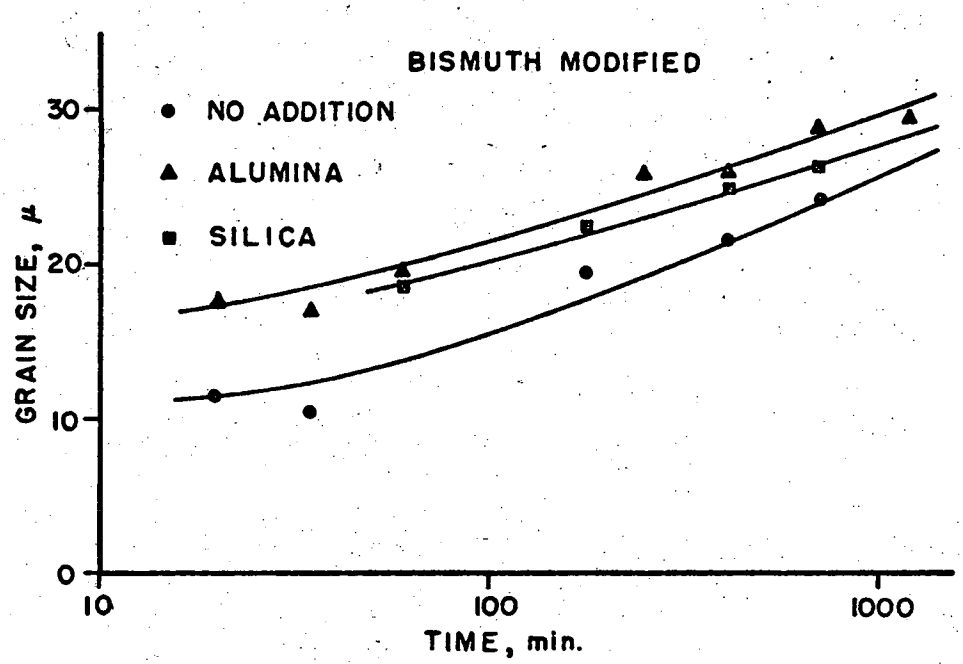

XBL 6812-6364

Fig. 7

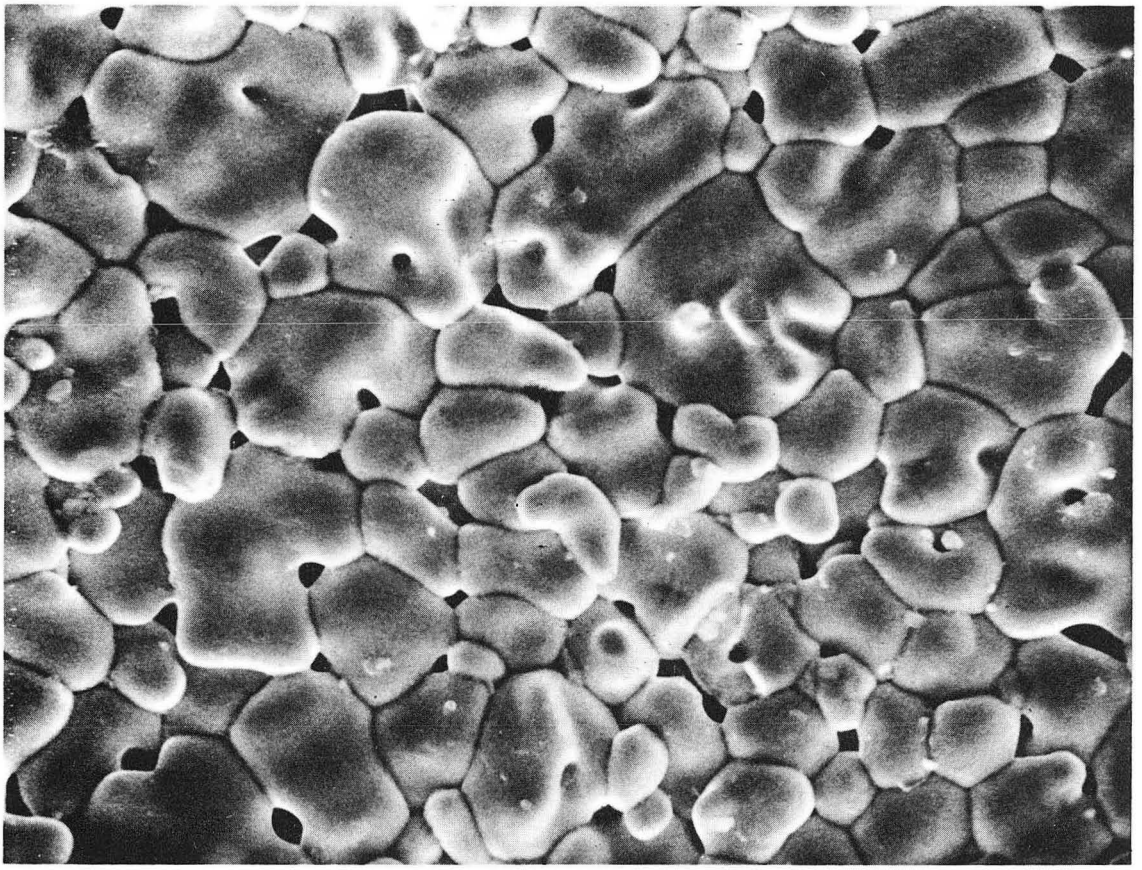

XBB 6810-6246

Fig. 8

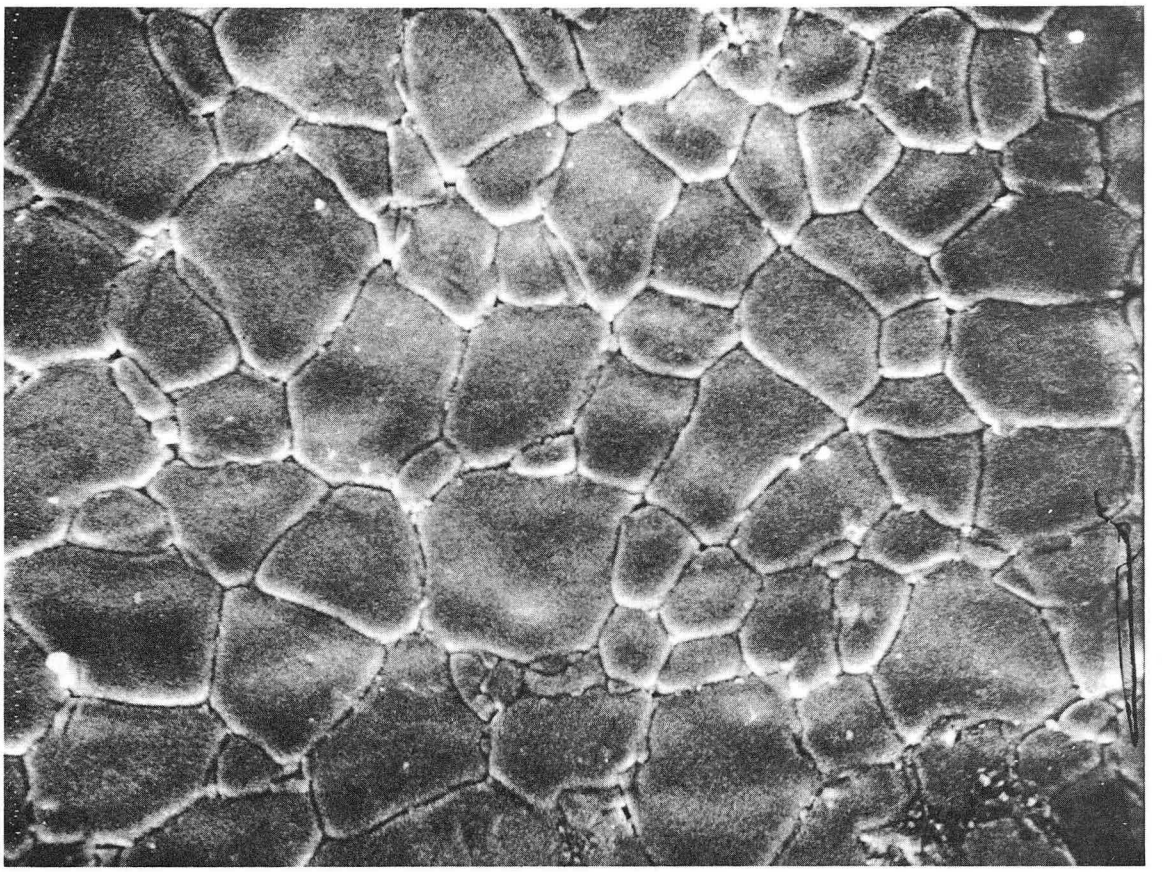

XBB 6810-6221

Fig. 9

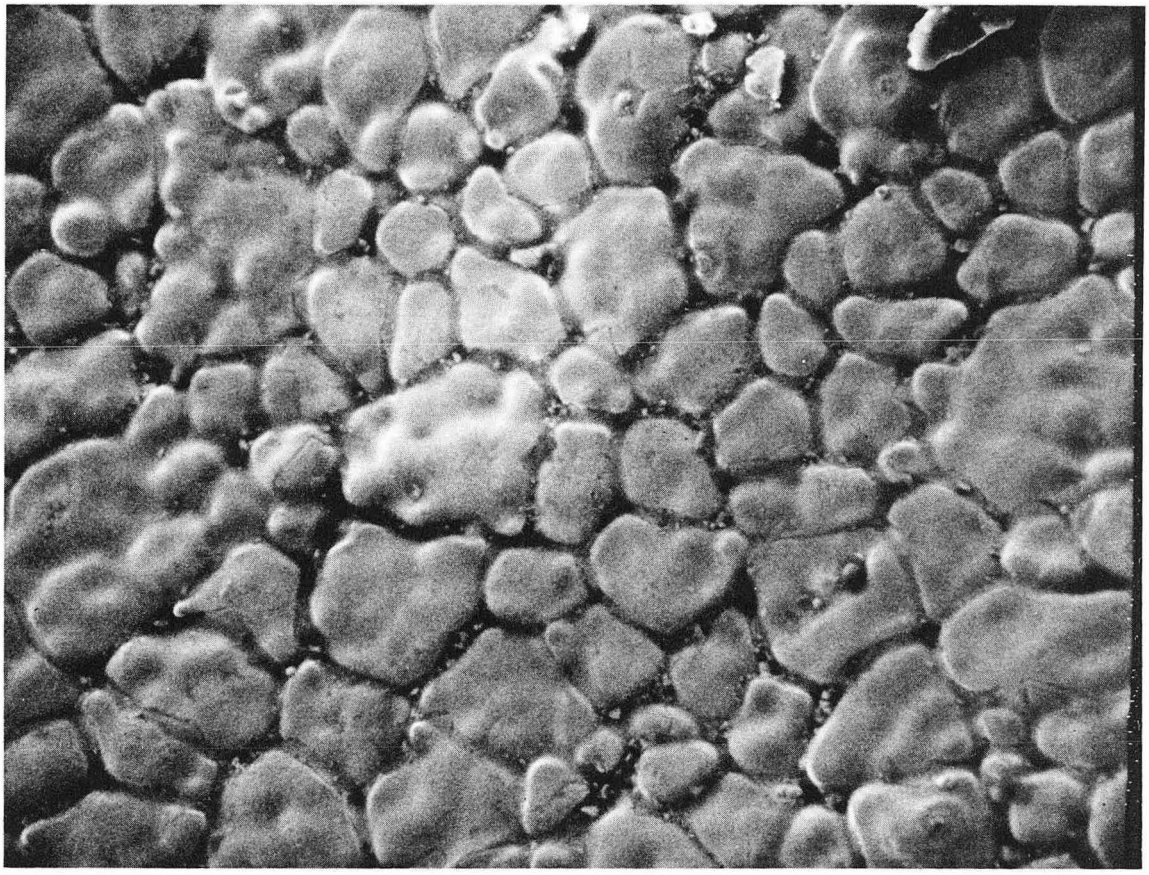

XBB 6810-6548

Fig. 10

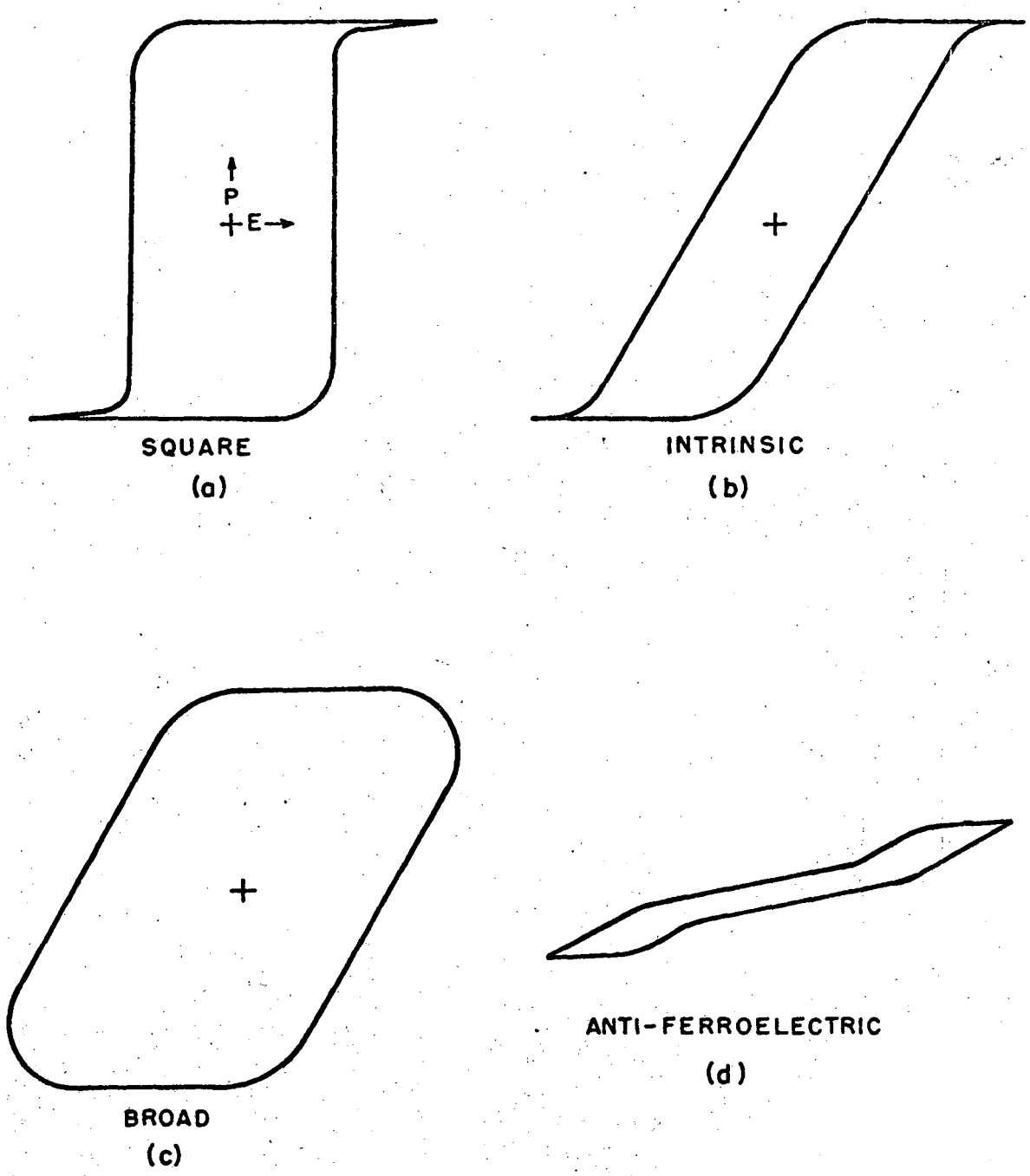

XBL 6812-6365

Fig. 11

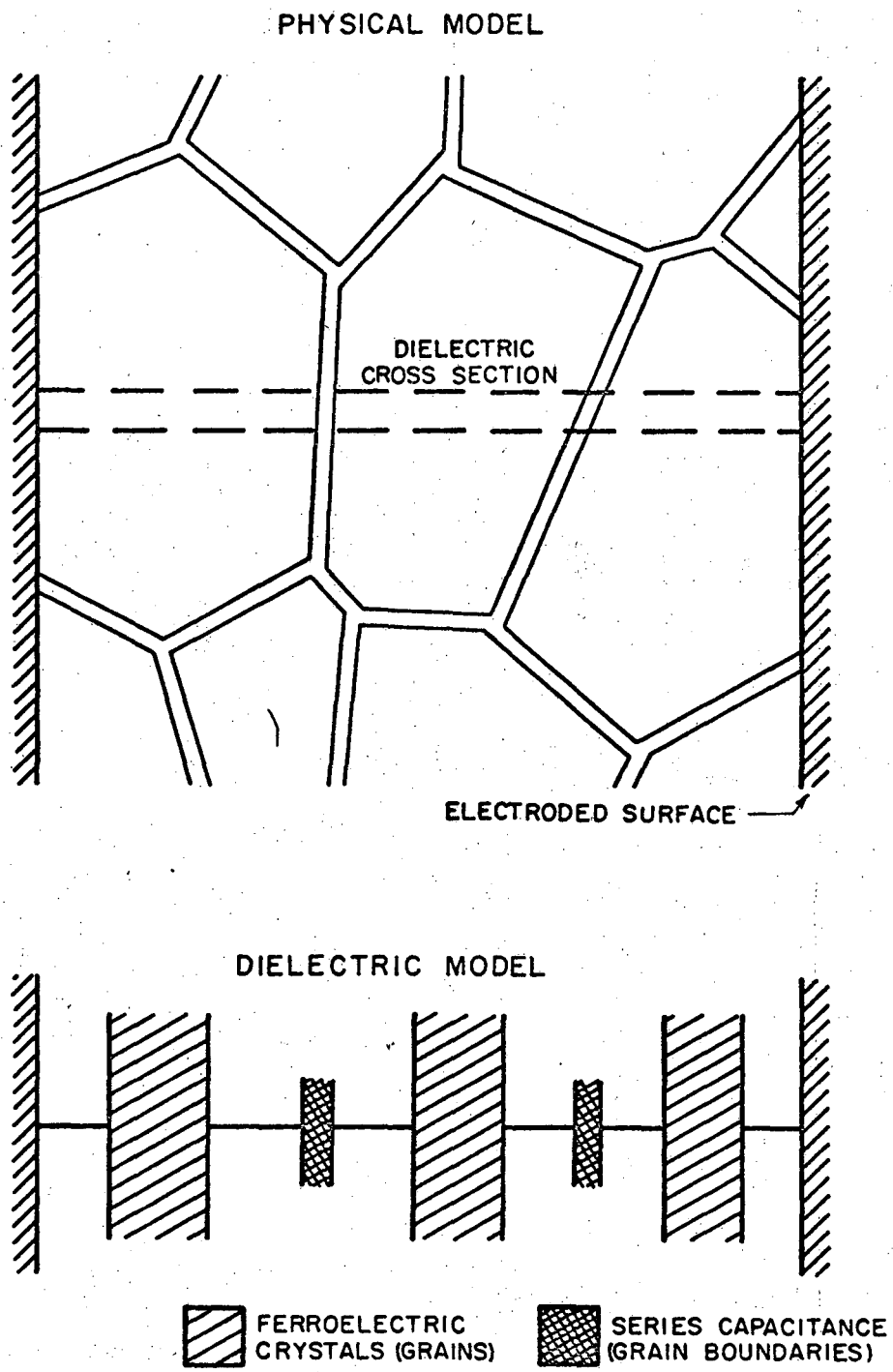

XBL 6812-6366

Fig. 12

LEGAL NOTICE

This report was prepared as an account of Government sponsored work. Neither the United States, nor the Commission, nor any person acting on behalf of the Commission:

A. Makes any warranty or representation, expressed or implied, with respect to the accuracy, completeness, or usefulness of the information contained in this report, or that the use of any information, apparatus, method, or process disclosed in this report may not infringe privately owned rights; or

B. Assumes any liabilities with respect to the use of, or for damages resulting from the use of any information, apparatus, method, or process disclosed in this report.

As used in the above, "person acting on behalf of the Commission" includes any employee or contractor of the Commission, or employee of such contractor, to the extent that such employee or contractor of the Commission, or employee of such contractor prepares, disseminates, or provides access to, any information pursuant to his employment or contract with the Commission, or his employment with such contractor.

TECHNICAL INFORMATION DIVISION
LAWRENCE RADIATION LABORATORY
UNIVERSITY OF CALIFORNIA
BERKELEY, CALIFORNIA 94720